

Paper No.
16653



Use of Quartz Crystal Microbalance in Study of Inhibitor Adsorption

Kushal Singla ^a, Hubert Perrot ^b, Ozlem Sel ^b, Bruce Brown ^a, Srdjan Nestic ^a

^aInstitute for Corrosion and Multiphase Technology (ICMT), Department of Chemical & Biomolecular Engineering, Ohio University, Athens, OH 45701

^bSorbonne Université, CNRS, Laboratoire Interfaces et Systèmes Electrochimiques (LISE, UMR 8235), 4 place Jussieu, (case courrier 133), F-75005, Paris, France

ABSTRACT

Although inhibitor adsorption and inhibition mechanisms have been studied extensively using various electrochemical techniques, these electrochemical techniques only provide an indirect estimate of inhibitor adsorption. Quartz crystal microbalance (QCM) has been shown to be a powerful acoustic technique which can be effectively used to evaluate net mass adsorption of inhibitors, adsorption rates and kinetic coefficients. In the present study, calibration of QCM by electrochemical deposition of copper on gold-coated quartz crystal resonator was done to evaluate the minimum mass change that can be determined using these devices. Sensitivity coefficient was measured within 5% accuracy for QCM-D equipment vs. within 20% accuracy for oscillatory circuit based-QCM equipment. Also, a different oscillatory circuit based-QCM equipment was used with flow cell to investigate the adsorption of tetra-decyl-dimethyl-benzyl-ammonium (Q-C14) inhibitor model compound on gold-coated quartz crystal resonator. Analysis of experimental data indicated that the inhibitor was adsorbed on the gold surface within a few minutes and the net amount of inhibitor adsorbed depends upon the bulk inhibitor concentration. However, the rate of frequency change for adsorption and desorption processes did not vary much for two inhibitor concentrations (50 ppm(w) and 100 ppm(w)) used for this study. This calls for further investigation of inhibitor adsorption at different concentrations.

Keywords: QCM, organic inhibitor, inhibitor adsorption, mass calibration, Sauerbrey equation

INTRODUCTION

Corrosion is a material degradation process, mostly related to metals, after exposure to adverse environmental conditions.¹ It leads to huge economic losses, environmental damage and

© 2021 Association for Materials Protection and Performance (AMPP). All rights reserved. No part of this publication may be reproduced, stored in a retrieval system, or transmitted, in any form or by any means (electronic, mechanical, photocopying, recording, or otherwise) without the prior written permission of AMPP.

Positions and opinions advanced in this work are those of the author(s) and not necessarily those of AMPP. Responsibility for the content of the work lies solely with the author(s).

possible risks to human life. According to a report published in 2016, economic losses due to corrosion were estimated to be US\$ 2.5 trillion which is approximately equivalent to 3.4% of the global Gross Domestic Product (2013).² Corrosion of carbon steel pipelines in oil and gas industry is a major contributor to corrosion related losses.² The majority of oil and gas transportation structures are made of low alloy carbon steel, which has poor resistance to corrosion. Hence, pipelines are often prone to internal corrosion in service environments. Any structural failure directly implies significant economic burdens and associated risk to the environment and human life. Therefore, corrosion as a process, becomes a key factor in structural design and material selection in energy applications.

The two main strategies to combat the problem of internal corrosion in upstream oil and gas pipelines are the use of corrosion resistant alloys and the addition of corrosion inhibitors to flow in mild steel pipelines. Corrosion resistant alloys (CRAs) are normally used in areas where inhibition of mild steels may not provide sufficient protection from corrosion related damages as the use of CRAs is typically not cost effective. Use of corrosion inhibitors is a comparatively cost effective corrosion mitigation method.^{3,4} A corrosion inhibitor (CI) is a chemical substance that, when added in small amounts, can diminish corrosion rates significantly in particular environments.¹ Development of CIs with high efficiency as well as persistency can yield huge advantages in saving corrosion costs.

Organic CIs are most widely used in the oil and gas industry. They are typically surfactant-type carbon-based compounds with a hydrophilic head group and a hydrophobic alkyl tail. It is a well-established fact that corrosion inhibition using organic CIs heavily relies on the mechanisms related to adsorption of molecules on a metal surface.^{3,5} However, the exact adsorption mechanisms are not yet clearly understood. Most of the research related to designing new inhibitor compounds has been based on trial and experimentation methods.¹ To design new CIs with increased efficiency, understanding their adsorption mechanisms is highly important. Many studies explain the process of corrosion inhibition using a “geometric blockage” model, which suggests the formation of a CI protective layer over the metal surface.^{3,6} This model suggests that CI’s work by forming a barrier layer between the metal surface and the water molecules, thus stopping corrosion by a blockage effect. The point of view of the “blockage model”, as discussed by Dominguez, *et al.*, contains intrinsic limitations that has hindered the development of a mechanistic model to satisfactorily describe and predict the effect of organic CIs on CO₂ corrosion of mild steel for many years.^{7,8} In 2016, Dominguez, *et al.*, has shown the ability to mechanistically model the influence of an inhibitor on mild steel corrosion and, in 2018, published results showing the influence of increasing the alkyl tail length of an inhibitor molecule on corrosion mechanisms by using this model.^{7,9} Although studies are becoming more mechanistic in nature, the current literature available in this field is dominated by purely qualitatively described inhibition mechanisms, which necessitates the continued development of more rigorous inhibition models to be used for corrosion prediction.⁴

With a broader purpose to understand inhibitor performance, it is important to address the adsorption mechanisms for CIs. Quantifying CI adsorption kinetics would develop this understanding further and enhance the use of this knowledge for field applications. QCM can be effectively used to study surface phenomena and evaluate net mass adsorption of inhibitors, as well as adsorption rates and kinetic coefficients. Moreover, the recent advances in this technology (QCM with dissipation monitoring) allows characterization of the structure and the viscoelastic properties of the adsorbed layer.^{10,11} This technique has been widely used in the fields of protein adsorption and air quality monitoring but has been minimally applied in corrosion

related research.^{11–13} To use QCM effectively and accurately, it is very important to understand the fundamentals and working principles of this technique and efficiently apply those to CI containing systems. With an effort to quantify the operating boundaries of the equipment with repeatability, reproducibility, sensitivity and accuracy as key parameters, mass calibration of an electrochemical quartz crystal microbalance (EQCM) was conducted using electrodeposition of copper on gold-coated quartz crystal resonators (QCRs).

This paper consists of two parts. The first part focuses on mass calibration experiments conducted using copper electrodeposition on two different types of QCM equipment. Apart from comparing the mass sensitivities for these two QCM, the focus was also to accurately define the electrochemically and piezoelectrically active area of a resonator and define the correct methodology to conduct mass calibration of a QCM. The second part of the paper reports on the experimental results for corrosion inhibitor adsorption on gold-coated QCR, conducted using an oscillatory circuit based-QCM setup equipped with a flow cell.

EQUIPMENT

Experiments presented in this paper were done on different QCM equipment. So, for the quick reference and the ease of reading, this section is added. For the first part of this paper on the mass calibration of QCM, experimental methodology and results obtained using Stanford Research Systems* (SRS QCM200 – shown in Figure 1a, referred to as QCM system 1) and AW Sensors† (AWS X1 - shown in Figure 1b, referred to as QCM system 2) are compared and summarized. QCM system 1 consists of a QCM200 digital controller, QCM25 crystal oscillator and crystal holder. QCM system 2 consists of a X1 controller and an electrochemical cell. The second part of this paper is focused on measurement of inhibitor adsorption, and a lab-made QCM setup (oscillatory circuit based) (as shown in Figure 2, referred to as QCM system 3) was used.

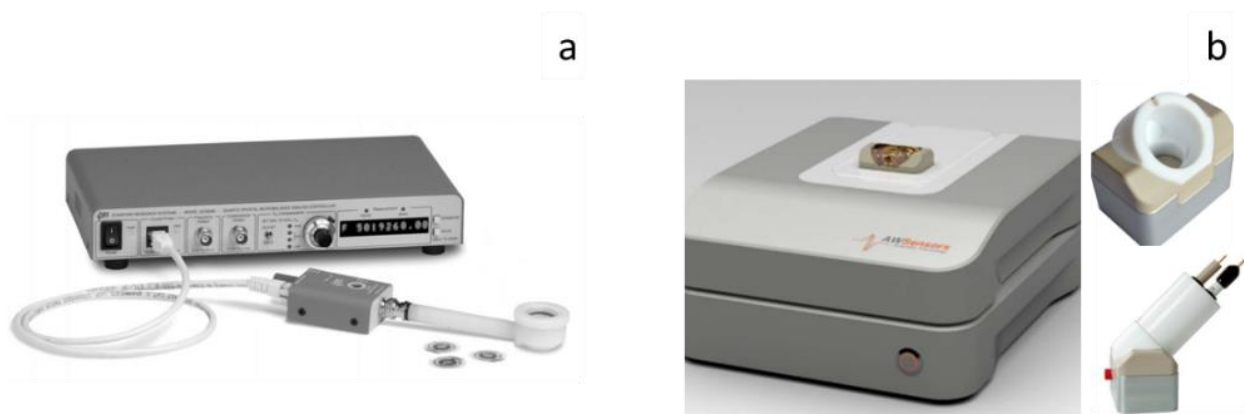


Figure 1: (a) The QCM200 setup consisting of digital controller, crystal oscillator and crystal holder.^{14,15} (Equipment based at ICMT, Ohio University and referred to as QCM system 1.) (b) The AWS X1 from AW sensors, setup consisting of controller and electrochemical cell.¹⁶ (Equipment based at LISE, Sorbonne University and referred to as QCM system 2.)

* Trade Name

† Trade Name

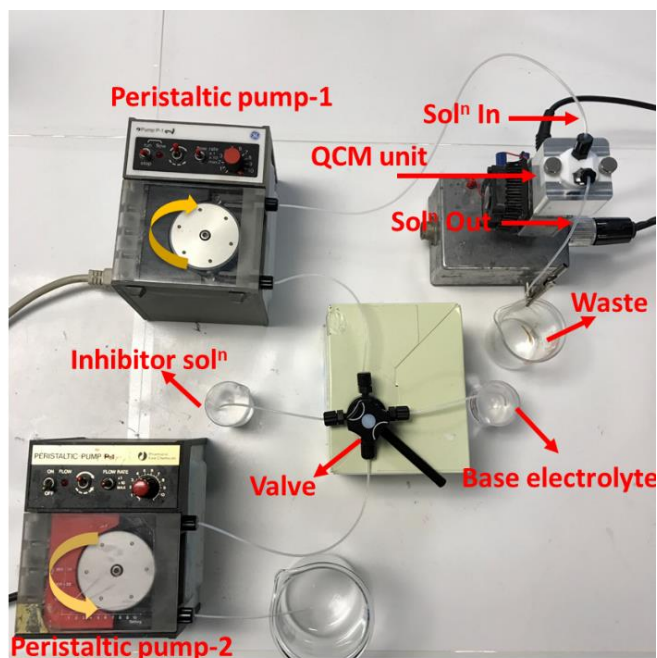


Figure 2: QCM setup equipped with flow cell used for inhibitor (Q-C14) adsorption. (Equipment based at LISE, Sorbonne University and referred to as QCM system 3.)

MASS CALIBRATION OF QCM

Methodology

The correct procedure for mass calibration was established and is as follows:

1. Calculate mass change using Faraday's law; variables: applied current (I) and time (t).

$$\Delta m_{Faraday} = \frac{I \cdot t \cdot M_w}{F \cdot n'} \quad (1)$$

where,

- $\Delta m_{Faraday}$ – mass deposited, g
- I – applied current, A
- t – time interval, s
- M_w – molar mass of substance, g mol⁻¹
- F – Faraday constant, 96485.3 C mol⁻¹
- n' – no. of electrons exchanged, $n'=2$

2. Evaluate piezoelectrically and electrochemically active area based on cell design and crystal configuration; A and A' respectively (measured in cm²).
3. Normalized electrochemically deposited mass based on Faradic calculations.

$$\Delta m_F = \frac{I \cdot t \cdot M_w}{F \cdot n'} * \left(\frac{A}{A'} \right) \quad (2)$$

where,

- Δm_F – normalized electrochemically deposited mass, g
- A' – electrochemically active area, cm²
- A – piezoelectrically active area, cm² (area of overlap between two electrodes)

4. Evaluate validity of Sauerbrey's equation; Δf vs. time.

5. Mass sensed by QCM (based on Sauerbrey's equation)^{10,17,18}

$$\Delta m_{QCM} = - \left(\frac{\left(\frac{\Delta f_{mass}}{n} \right)}{C_f} \right) * A \quad (3)$$

where,

$$C_f = -2f_o^2 (\mu_q \rho_q)^{-\frac{1}{2}} \quad (4)$$

μ_q - shear modulus for quartz crystal ($2.947 \times 10^{11} \text{ g cm}^{-1} \text{ s}^{-2}$)

ρ_q - density of quartz crystal (2.648 g/cm^3)

n - number of overtones

✓ In air, theoretical value of C_f for 5 MHz AT-cut quartz crystal is $56.6 \text{ Hz cm}^2 \mu\text{g}^{-1}$

✓ In air, theoretical value of C_f for 9 MHz AT-cut quartz crystal is $183.4 \text{ Hz cm}^2 \mu\text{g}^{-1}$

6. Compare equations (2) and (3) to get the experimental mass sensitivity value, C_f .

Electrochemically and piezoelectrically active area:

One key parameter that plays an important role in data analysis in the mass calibration procedures for the QCM is to evaluate the exact piezoelectric and electrochemically active areas. So, to shed clarity on this aspect, the two areas for three different QCR configurations and cell designs used (Figure 3) are explained in this section.

Figure 3 schematically shows the 3 different QCR configurations and the side view representation of their position in the experimental cells. The top part is in contact with electrolyte (represented here by sea green color, Figure 3) and this wetted electrode area will be referred to as the electrochemically active area (A'). The area of overlap between gold electrodes on two sides of quartz crystal is defined as the piezoelectrically active area (A). The solid boundaries on the top part and dashed boundaries on the bottom part are representative of experimental cell walls, in contact with the electrolyte and in air, respectively. A and A' is estimated and associated to the different configurations in the following part.

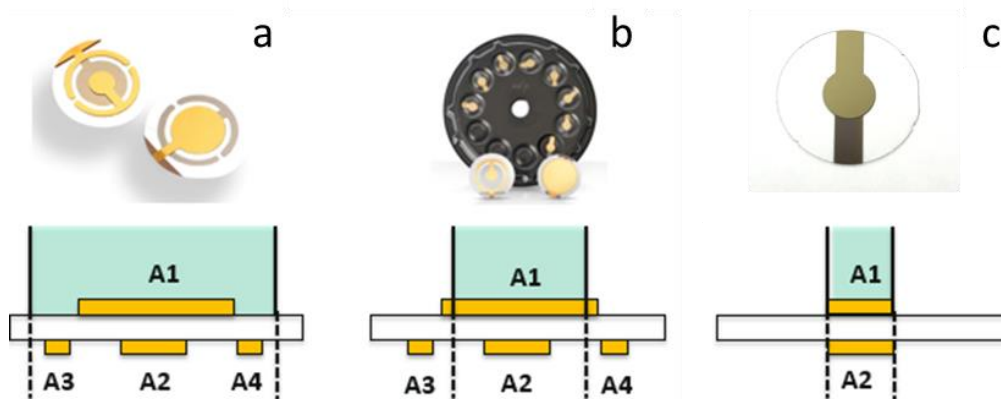


Figure 3: Different QCR configurations and schematic for QCR in experimental cell design. (a) Wrapped around configuration for QCM system 1.¹⁴ (b) Wrapped around configuration for QCM system 2.¹⁹ (c) Keyhole configuration for QCM system 3.

Evaluation of piezo and electrochemically active areas for each case:

- i. Wrapped around configuration (QCM system 1, Figure 3a):
 - a) Electrochemically active area: $A' \rightarrow A1$
 - b) Area of overlap between two electrodes: $A2$, but
 - c) Real piezoelectrically active area: $A \rightarrow A2 + A3 + A4$ (because for mass calibration experiments, a conducting solution is used, hence the electrode on the top of the QCR behaves as a continuous electrode spread over the entire wetted area and hence, the area of overlap becomes a summation of three areas ($A2$, $A3$ and $A4$))
 - d) $A1 = A2 + A3 + A4$
 - e) $A' = A$ ($= 1.38 \text{ cm}^2$ for QCM system 1)
- ii. Wrapped around configuration (QCM system 2, Figure 3b):
 - a) Electrochemically active area: $A' \rightarrow$ less than $A1$
 - b) Area of overlap between two electrodes: $A2$
 - c) Piezoelectrically active area: $A \rightarrow A2$
 - d) $A1 \neq A2$
 - e) $A' \neq A$; so, the exact piezoelectric and electrochemical area needs to be evaluated separately for mass calibration experiments conducted on QCM system 2.
 - f) A' is 0.93 cm^2 and A is 0.24 cm^2 for QCM system 2.
- iii. Keyhole configuration (QCM system 3, Figure 3c):
 - a) Electrochemically active area: $A' \rightarrow A1$
 - b) Area of overlap between two electrodes: $A2$
 - c) Piezoelectrically active area: $A \rightarrow A2$
 - d) $A1=A2$
 - e) $A' = A$ ($= 0.22 \text{ cm}^2$ for QCM system 3)

Testing Procedure

Figure 4 is the schematic of the experimental setup that was used for mass calibration experiments conducted on QCM system 1. The temperature of the system was controlled using a ceramic hot plate with a thermocouple feedback. Test conditions for this experiment are tabulated in Table 1. AT-cut gold coated, polished quartz crystals with a fundamental resonance frequency of ~ 5 MHz were used (Maxtek, #149211-1) as the working electrode. The copper layer was electrodeposited over a polished gold electrode surface by applying galvanostatic cathodic current using a galvanostat. QCM system 1 setup was used for exciting the crystal and monitoring the frequency and motional resistance data with time.¹⁵

Figure 5 shows the images of the electrochemical cell that was used for mass calibration experiments conducted at LISE. QCM system 2 has a built-in temperature control and the temperature during the experiments was maintained at 25°C . Test conditions for this experiment are shown in Table 2. AT-cut gold coated, polished quartz crystals with a fundamental resonance frequency of ~ 5 MHz were used (AWS SNS 000043 A). One of the gold electrode, in contact with the electrolyte, can act as a classical working electrode. A galvanostat was used for all electrodeposition procedures. First, a copper layer was electrogenerated over the polished gold electrode surface by applying a cathodic current of -1 mA for 20 s in the same testing solution as mentioned in Table 2. Then, the QCM response was measured for copper electrodeposition over an electrode which is already covered with electrogenerated copper. Frequency and dissipation response at different overtones were monitored in real time.

Table 1: Test matrix for galvanostatic electrodeposition of copper on gold coated, polished, 5 MHz quartz crystal resonator, QCM system 1.

Temperature	30 °C
pH	1.2
Solution	0.5 M H ₂ SO ₄ + 50mM CuSO ₄ ·5H ₂ O
Working electrode	Gold coated quartz crystal resonator (5MHz, polished)
Stirring	Off
Nitrogen purge	1 hour
Applied current	-0.5 mA, -1 mA and -2mA
Time (current applied for)	30 s
Electrochemical Cell	2L glass beaker, with Ag/AgCl reference electrode and platinum coated mesh as counter electrode

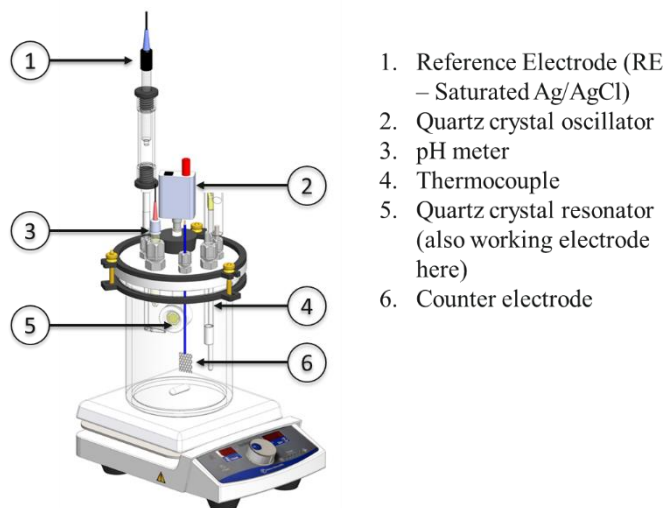


Figure 4: Experimental setup for galvanostatic electrodeposition of copper on Au coated quartz crystal resonator (5MHz, polished). (Image Courtesy: Cody Shafer, ICMT)

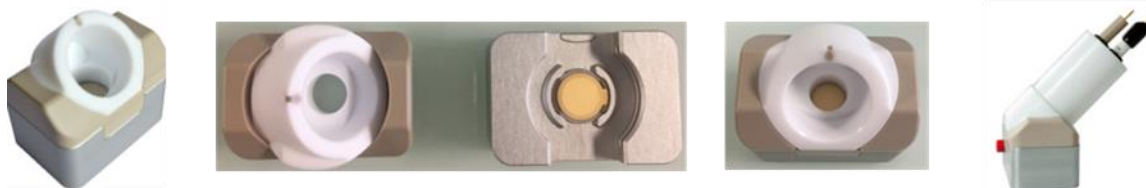


Figure 5: QCM system 2 with electrochemical cell, used for galvanostatic electrodeposition of copper on Au coated quartz crystal resonator (5MHz, polished).¹⁶

Table 2: Test matrix for galvanostatic electrodeposition of copper on gold coated, polished, 5 MHz quartz crystal resonator, QCM system 2.

Temperature	25 °C
Solution	0.1 M H ₂ SO ₄ + 0.5 M CuSO ₄ .5H ₂ O
Working electrode	Gold coated quartz crystal resonator (5MHz, polished)
Applied current	-0.5 mA, -0.75 mA and -1mA
Time (current applied for)	30 s
Electrochemical Cell	As shown in Figure 5, with Ag/AgCl reference electrode and platinum wire as counter electrode

Copper Electrodeposition Experiments

The aim of these experiments was to evaluate the repeatability, accuracy, and mass sensitivity of QCM equipment by copper electrodeposition. As explained previously, mass sensed by QCM (Equation (3)) will be compared to normalized electrochemically deposited mass (Equation (2)). Observing a linear relationship of frequency change with time at different cathodic current values indicates a linear relation between frequency change and mass change; hence approves the applicability of Sauerbrey's equation.¹⁷

Comparing frequency change with respect to time:

Figure 6 (a) and (b) shows the variation of frequency change with respect to time for copper electrodeposition on Au coated 5 MHz QCR. It is evident from Figure 6 (a) and (b) that a linear relationship between frequency change and time is valid for all the different cathodic currents applied. So, by this way, it is possible to calculate QCM sensitivity. It is also important to mention here that frequency change for QCM system 1 and QCM system 2 is equivalent but not same for the same current value and time. This is because the electrochemically and piezoelectrically active areas are different for two QCM systems as explained previously.

The major difference however between QCM system 1 and QCM system 2 is the ability of QCM system 2 to monitor frequency change simultaneously for different overtones. Figure 7 show the frequency response captured by QCM system 2 at multiple overtones (i.e. n=1,3,5,7 and 9) for cathodic currents of -0.5 mA. Similar behavior was observed for cathodic currents of -0.75 mA and -1 mA. Frequency response for different overtones overlaps perfectly for a value of cathodic current. Overlapping of frequencies at multiple overtones is a clear indication of uniform deposition of copper layer over the QCR, which fulfils another basic requirement for the application of Sauerbrey's equation. Earlier for QCM system 1, based on linear response of frequency with time, it was established that Sauerbrey's equation was valid while analyzing data. But, due to the limitations of the equipment (single frequency measurements) there was no possible way to comment on the uniformity of the deposited layer. However, using QCM system 2, frequency change data is captured for multiple overtones simultaneously which provides more insights about the deposited layer properties and hence provides more confirmation on the validity of the Sauerbrey's equation.

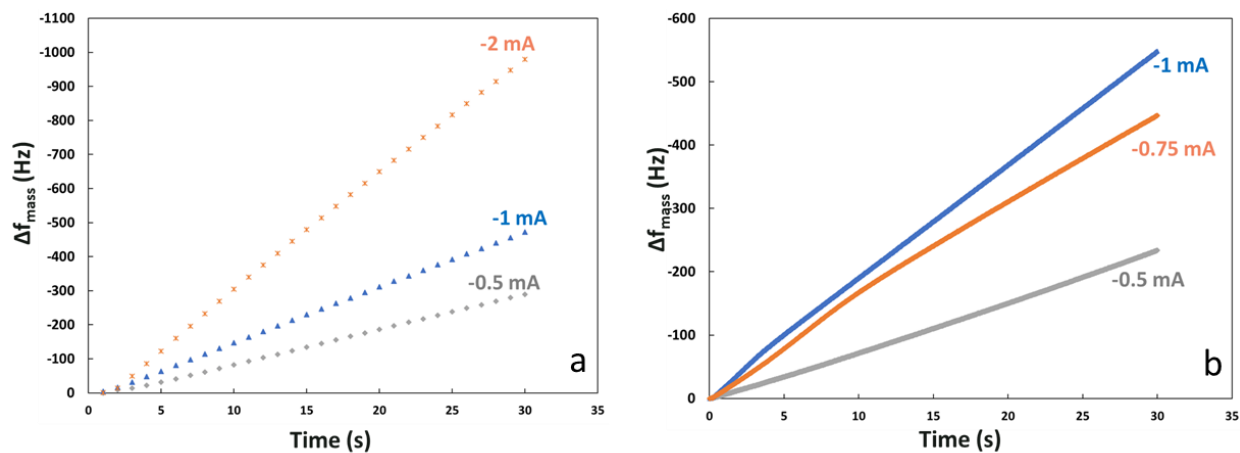


Figure 6: Time variation of the EQCM frequencies for different cathodic currents measured using (a) QCM system 1, (b) QCM system 2 for the fundamental frequency, 1st overtone, i.e. n=1.

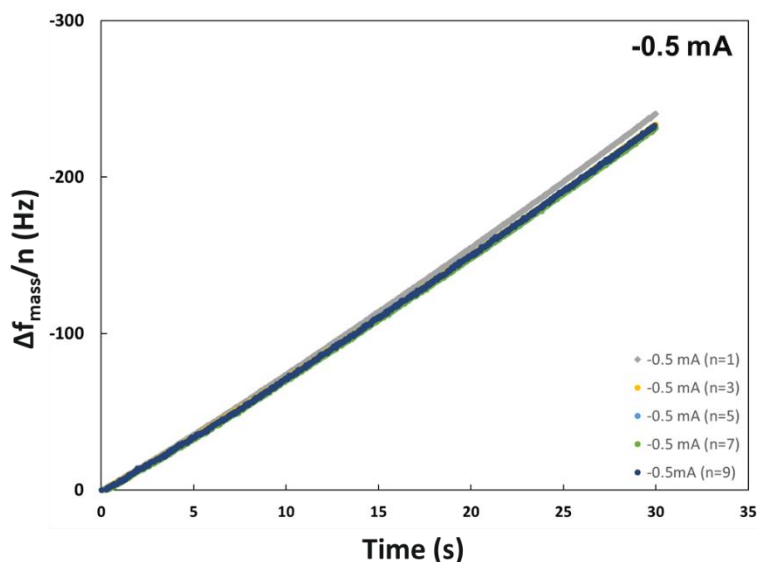


Figure 7: Time variation of the EQCM frequencies monitored at multiple overtones simultaneously for -0.5 mA cathodic current, LISE equipment (QCM system 2).

Comparing mass change per unit area (Faraday's law vs. Sauerbrey's equation):¹⁷

Figure 8 (a) and (b) show parity plots where the y-axis is experimental mass change for electrodeposition of copper calculated using Sauerbrey's equation (Equation (3)) and the x-axis is theoretical mass change calculated using Faraday's law (Equation (2)). The blue line represents an ideal case scenario where all experimental values will match perfectly with theoretical calculations. By comparison it was found that accuracy of the copper electrodeposition experiments lies within 20% of the theoretical calculations for QCM system 1 and lies within 5% of the theoretical calculations for QCM system 2. It should be noted here that in the accuracy offset values for two QCM systems, there might be a contribution of the efficiency of copper reduction reaction. For the experiments in this paper, it is assumed that 100% of the applied cathodic current is being used for copper reduction reaction which might not be the actual scenario and hence the offset from theoretical line. Also, for experiments on QCM system 2,

copper was electrodeposited over a layer of copper as compared to copper over gold electrodeposition for experiment done on QCM system 1. This can also be a contributing factor to improved results for QCM system 2. Therefore, it is recommended to deposit copper over an already electrodeposited copper layer on QCR as a standard practice for carrying out mass calibration of QCM.

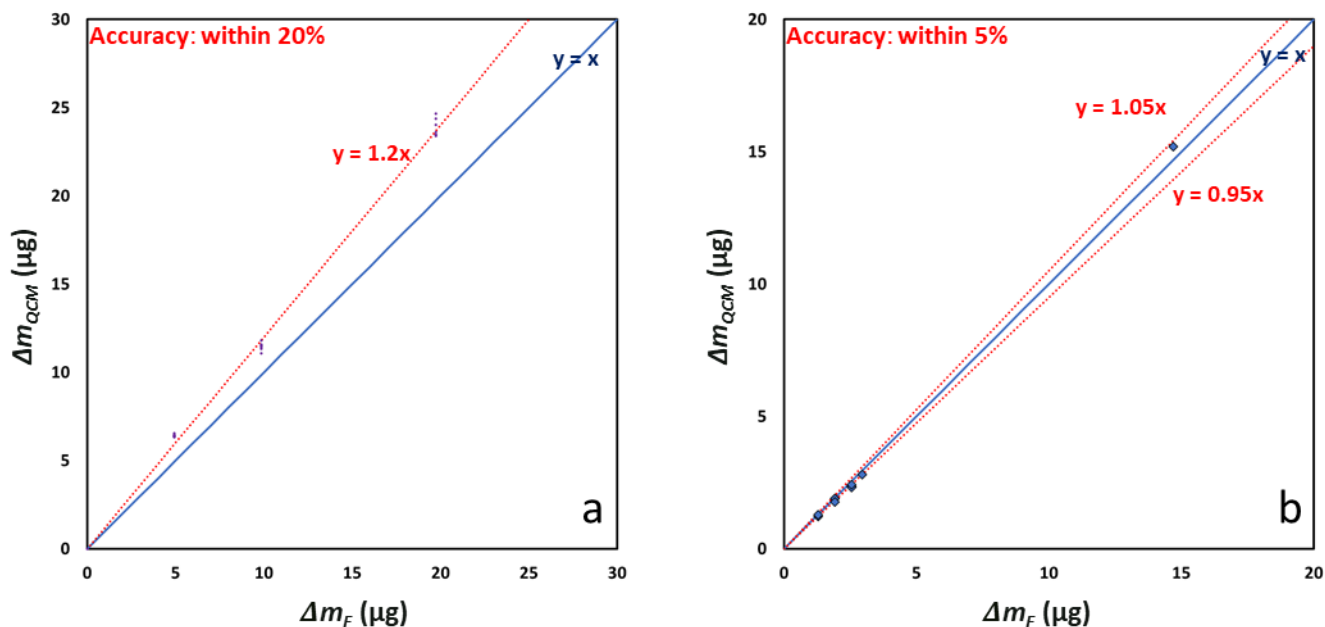


Figure 8: Parity plot comparing mass change for copper electrodeposition experiments using QCM with y-axis representing Sauerbrey's equation calculations and x-axis representing calculations using Faraday's law of electrolysis. (a) QCM system 1 and (b) QCM system 2.

Findings for Mass Calibration of QCM

- i. Piezo and electrochemically active area: Evaluating the relationship between these two areas is the key step and this depends upon the configuration of QCR's and cell design.
- ii. Frequency change response vs. time
 - a. For electrochemical deposition of copper on QCR, the frequency change has a linear response with respect to time.
 - b. Linear frequency response vs. time at multiple harmonics using QCM system 2 also signified that copper deposit on QCR can be considered as a rigid and uniform mass deposit and hence approves the validity of Sauerbrey's equation for this experimental system.
- iii. Sensitivity coefficient (C_f) was measured within **5% accuracy** for QCM system 2 vs. **20% accuracy** measured using QCM system 1.
 - a. Measured C_f for:
 - QCM system 1 is: $56.6 \pm 11.3 \text{ Hz cm}^2 \mu\text{g}^{-1}$
 - QCM system 2 is: $56.6 \pm 2.8 \text{ Hz cm}^2 \mu\text{g}^{-1}$
 - b. Depositing **copper over gold** vs. depositing **copper over copper** can also be a major contributing factor for improved results for QCM system 2.

INHIBITOR ADSORPTION (Q-C14) USING AN OSCILLATORY CIRCUIT BASED QCM SETUP EQUIPPED WITH A FLOW CELL

Experimental Procedure

Figure 2 shows experimental setup that was used for inhibitor adsorption experiments on QCM system 3 with a flow cell. Model corrosion inhibitors such as quaternary ammonium-based compounds and imidazolines with different alkyl tail lengths have been synthesized at lab scale as a part of another project at the ICMT. The rationale of using lab synthesized model compounds was to decrease the number of unknowns in the experiments because it is understood that commercial CI packages contain certain formulations which are trade secrets.^{1,5} For this study, adsorption behavior of a quaternary ammonium type corrosion inhibitor, Q-C14, is tested. Test conditions for this experiment are tabulated in Table 3. AT-cut gold coated, polished quartz crystals with a fundamental resonance frequency of ~9 MHz were used (AWS SNS 000019 C) as the substrates. The QCM unit monitors frequencies at the 3rd overtone, i.e. change in frequency was measured with respect to 27 MHz.¹⁸ Two peristaltic pumps were used for flow of solutions and a 4-way valve was used to switch between two solutions (base electrolyte and inhibitor solution). Firstly, base electrolyte without any inhibitor was pumped through the QCM cell at a constant flow rate to get the baseline frequency response against which any change in frequency due to mass adsorption was measured. Then, the valve was switched to flow inhibitor solution through the QCM cell and the change in frequency was measured with respect to time until it reached a stable value. This cycle was repeated to collect adsorption/desorption curves represented in terms of normalized frequency change ($\Delta f/3$) w.r.t. time for inhibitor solutions with inhibitor concentrations of 50 ppm(w) and 100 ppm(w).

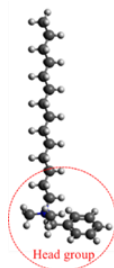


Figure 9: Tetradecylbenzyltrimethylammonium (Q-C14); a quaternary ammonium-type corrosion inhibitor.²⁰

Table 3: Test matrix for inhibitor (Q-C14) adsorption on gold coated, polished, 9 MHz quartz crystal resonator using QCM system 3 with flow cell.

Base Electrolyte	1 wt. % NaCl in deionized water
Inhibitor Solution	100 ppm(w) & 50 ppm(w) Q-C14* in base electrolyte
Substrate/QCR	9 MHz, keyhole configuration, Au/Ti, polished
Operating overtone	n=3
Flow rate	0.05 ml/minute

* Q-C14: tetra-decyl-dimethyl-benzyl-ammonium bromide

Results and Discussion

The aim of these experiments was to quantify the inhibitor adsorption via measuring a change in resonance frequency using a QCM. Expectations:

- i. Stable, repeatable, and reproducible frequency response with respect to time for base solution to have a baseline frequency.
- ii. Repeatable and quantifiable change in frequency while using inhibitor solution. The results can be analyzed for *net frequency change* and *rate of change of frequency with time* with the introduction of inhibitor solution.
- iii. Difference in mass adsorption rates and net inhibitor mass adsorbed for two different concentrations of inhibitor used for experiments (50 ppm(w) and 100 ppm(w)).

Please note that for the present paper, frequency values were converted into mass using Sauerbrey's equation (Equation (3)) and using C_f of $183.4 \text{ Hz cm}^2 \mu\text{g}^{-1}$ to give a rough estimate for adsorbed layer mass.^{17,18} This approach and the applicability of Sauerbrey interpretation to the present system needs to be validated, given the fact that adsorbed layer properties (rigid or viscoelastic, etc.) are not known. Moreover, it is not possible to comment about the properties of the adsorbed layer using only frequency data recorded at a single overtone. In most likelihood, the adsorbed inhibitor layer is viscoelastic in nature i.e. not a rigid mass deposit, hence the use of Sauerbrey's equation in this scenario might lead to over or underestimation of the real mass changes.²¹ Further studies should include multi-harmonic QCM measurements with dissipation monitoring or electroacoustic admittance measurements and data analysis with viscoelastic modelling. It should also be noted here that inhibitor adsorption experiments for this study were carried out on gold coated QCR rather than on iron. This is done to avoid the complexity of a possible contribution to the frequency change due to corrosion of iron. Considering gold as an inert surface, setting aside the applicability of Sauerbrey's equation as explained above, any frequency change from a gold-coated QCR in an inhibitor containing solution is related to adsorption/desorption of inhibitors. Xiong, *et al.*, found that an imidazolium-type organic inhibitor molecule provided consistent adsorption properties on mica, gold, and steel surfaces as measured by atomic force microscopy indicating that experimentation with different materials can provide a valid approach to understanding adsorption mechanisms.²² However, since the final application of inhibitors is on steel, authors would also compare and address the relationship between the adsorption/desorption of QC-14 on gold-coated QCR to a carbon steel surface in future studies.

As explained earlier in the methodology, once the baseline was reached for resonance frequency vs. time, the valve was switched between the two solutions, inhibitor solution and base electrolyte, to get the adsorption and desorption characteristics. Also, the points shown in Figure 10 (a) and (b) are not the actual experimental points but the moving averages of ten experimental points. The frequency response for individual experiments was combined in Figure 10 to show an overall adsorption/desorption curve which will be of more use for understanding the adsorption behavior. Any decrease in frequency refers to adsorption because when mass gets adsorbed on QCR, the resonance frequency will decrease. Similarly, any increase in frequency value refers to desorption of inhibitor molecules from QCR surface. Consequently, net frequency change and rate of frequency change can be quantified. Moreover, the inhibitor adsorption process is reversible at inhibitor concentrations used for the experiments (50 ppm(w) and 100 ppm(w)). The reversibility of the adsorption/desorption process can be clearly related to frequency change values which returns to baseline frequency during the desorption step as

can be seen in Figure 10 (a) and (b). Table 4 summarizes the same results with corresponding mass calculations using Sauerbrey's equation.

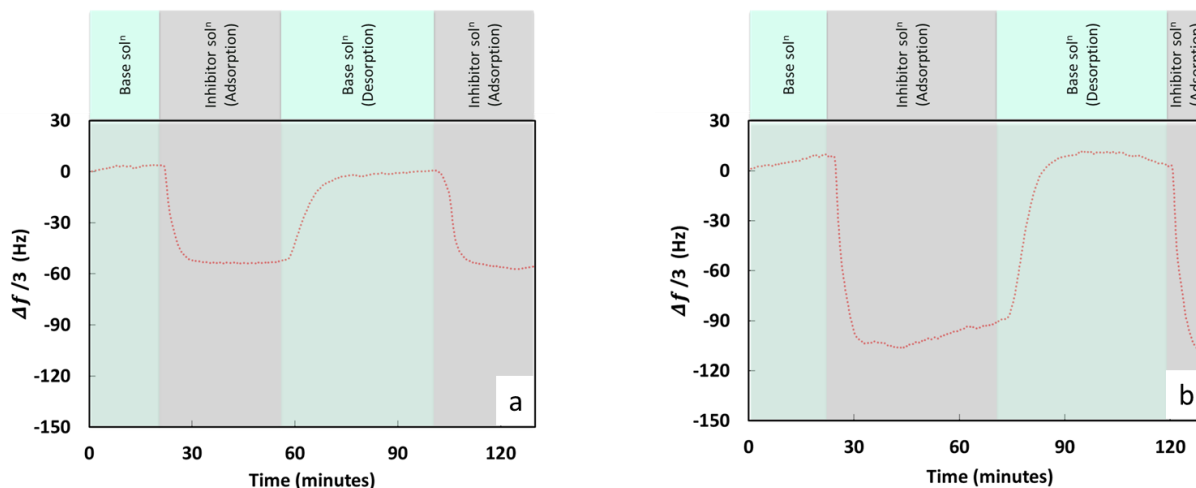


Figure 10: Normalized frequency change vs. time for inhibitor concentration of (a) 50 ppm(w), combined plot for three experiments and (b) 100 ppm(w), combined plot for three experiments.

Table 4: Results summary for inhibitor adsorption experiments.

Parameter	Average value	
	50 ppm(w)	100 ppm(w)
Δf (Hz)	65 ± 14	93.3 ± 14
Δm_{QCM} (ng)	~70	~100
Rate of change of frequency for adsorption step (Hz/min)	5.5 ± 2	10.1 ± 4
Adsorption rate (nanomoles/cm ² *min)	0.09 ± 0.03	0.16 ± 0.06
Rate of change of frequency for desorption step (Hz/min)	6.1 ± 1.5	8.2 ± 2
Desorption rate (nanomoles/cm ² *min)	0.1 ± 0.02	0.13 ± 0.03

Conclusions

The key takeaways from these experiments are:

- i. Average inhibitor adsorption increased with increasing inhibitor concentration.
- ii. Average inhibitor adsorption and desorption rates were within close range of each other for two inhibitor concentrations used.
- iii. With the current data, frequency changes are converted to mass variations using Sauerbrey's equation which provided an initial estimation. Future studies should focus on deconvoluting the various factors that might have been contributing to frequency change.

ACKNOWLEDGEMENTS

The authors would like to thank the following companies for their financial support: Baker Hughes, BP, Chevron, Clariant Corporation, CNOOC, ConocoPhillips, ExxonMobil, M-I SWACO (Schlumberger), Multi-Chem (Halliburton), Occidental Oil Company, Pioneer Natural Resources, Saudi Aramco, Shell Global Solutions, SINOPEC (China Petroleum), and TOTAL.

REFERENCES

1. Fontana, M. G. *Corrosion engineering*. (McGraw-Hill, 2010).
2. Koch, G. *et al. International Measures of Prevention , Application , and Economics of Corrosion Technologies Study. NACE International* (2016).
3. McCafferty, E. *Introduction to corrosion science*. (Springer, 2010).
4. Cao, C. On Electrochemical Techniques for Interface Inhibitor Research. *Corros. Sci.* **38**, 2073–2082 (1996).
5. Sastri, V. S. *Green Corrosion Inhibitors: Theory and Practice*. (John Wiley & Sons, 2011). doi:10.1002/9781118015438.
6. Jones, D. A. *Principles and Prevention of Corrosion. Prentice Hall International, Inc.* (1997). doi:10.1016/0261-3069(93)90066-5.
7. Olivo, J. M. D., Brown, B. & Nescic, S. Modeling of Corrosion Mechanisms in the Presence of Quaternary Ammonium Chloride and Imidazoline Corrosion Inhibitors. in *NACE Corrosion Conference 7406* (2016).
8. Domínguez Olivo, J. M., Brown, B., Young, D. & Nešić, S. Electrochemical model of CO₂ corrosion in the presence of quaternary ammonium corrosion inhibitor model compounds. in *NACE Corrosion Conference 13392* (2019).
9. Domínguez Olivo, J. M., Brown, B., Young, D. & Nešić, S. Effect of Corrosion Inhibitor Alkyl Tail Length on the Electrochemical Process Governing CO₂ Corrosion of Mild Steel. in *NACE Corrosion Conference* (2018).
10. Dixon, M. C. Quartz crystal microbalance with dissipation monitoring: Enabling real-time characterization of biological materials and their interactions. *J. Biomol. Tech.* **19**, 151–158 (2008).
11. Johannsmann, D. *The Quartz Crystal Microbalance in Soft Matter Research*. (Springer, 2015). doi:10.1007/978-3-319-07836-6.
12. Hepel, M. Electrode-Solution Interface Studied with Electrochemical Quartz Crystal Nanobalance. *Interfacial Electrochem. Theory Exp. Appl.* 599–630 (1999).
13. Deakin, M. R. & Buttry, D. A. Electrochemical Applications of the Quartz Crystal Microbalance. *Anal. Chem.* **61**, 1147 A-1154 A (1989).
14. ICMT Equipment and Instrumentation.

<https://www.ohio.edu/engineering/corrosion/facilities-equipment/equipment.cfm>.

15. *Operations and Service Manual-QCM200 Quartz Crystal Microbalance. Technical Reports* (2004).
16. AWSensors. AWS X1 Product Brouchre. 1–6 (2019).
17. Gabrielli, C., Keddam, M. & Torresi, R. Calibration of the Electrochemical Quartz Crystal Microbalance. *J. Electrochem. Soc.* **138**, 2657–2660 (1991).
18. Bizet, K., Gabrielli, C. & Perrot, H. Immunodetection by quartz crystal microbalance: A new approach for direct detection of rabbit IgG and peroxidase. in *Applied Biochemistry and Biotechnology - Part A Enzyme Engineering and Biotechnology* vol. 89 139–149 (Springer, 2000).
19. AWSensors. AWS Product Catlogue. 1–20 (2018).
20. Hanwell, M. D. *et al.* Avogadro: An advanced semantic chemical editor, visualization, and analysis platform. *J. Cheminform.* **4**, 113 (2012).
21. Solin, K. *et al.* Electrically Conductive Thin Films Based on Nanofibrillated Cellulose: Interactions with Water and Applications in Humidity Sensing. *ACS Appl. Mater. Interfaces* **12**, 36437–36448 (2020).
22. Xiong, Y., Brown, B., Kinsella, B., Nešić, S. & Pailleret, A. Atomic force microscopy study of the adsorption of surfactant corrosion inhibitor films. *Corrosion* **70**, 247–260 (2014).